Garlic-Derived *S*-allylmercaptocysteine Is a Novel *In vivo* Antimetastatic Agent for Androgen-Independent Prostate Cancer

Edward W. Howard, Ming-Tat Ling, Chee Wai Chua, Hiu Wing Cheung, Xianghong Wang, and Yong Chuan Wong

Abstract

Purpose: There is epidemiologic evidence that high garlic consumption decreases the incidence of prostate cancer, and compounds isolated from garlic have been shown to have cancer-preventive and tumor-suppressive effects. Recent *in vitro* studies in our laboratory have shown that garlic-derived organosulfur compound *S*-allylmercaptocysteine suppresses invasion and cell motility of androgen-independent prostate cancer cells via the up-regulation of cell-adhesion molecule E-cadherin. *S*-allylmercaptocysteine is therefore a potential antimetastatic drug with broad clinical applications that we tested *in vivo* for the first time in this study.

Experimental Design: We used a newly established fluorescent orthotopic androgen-independent prostate cancer mouse model to assess the ability of *S*-allylmercaptocysteine to inhibit tumor growth and dissemination.

Results: We showed that oral *S*-allylmercaptocysteine not only inhibited the growth of primary tumors by up to 71% ($P < 0.001$) but also reduced the number of lung and adrenal metastases by as much as 85.5% ($P = 0.001$) without causing notable toxicity. This metastatic suppression was accompanied by a 91% reduction of viable circulating tumor cells ($P = 0.041$), suggesting that *S*-allylmercaptocysteine prevents dissemination by decreasing tumor cell intravasation.

Conclusions: Our results provide *in vivo* evidence supporting the potential use of *S*-allylmercaptocysteine as an E-cadherin up-regulating antimetastatic agent for the treatment of androgen-independent prostate cancer. This is the first report of the *in vivo* antimetastatic properties of garlic, which may also apply to other cancer types.

Prostate cancer is the second most frequent cause of male cancer death in the United States (1). Despite the widespread presence of clinically insignificant tumors in elderly men, prostate cancer commonly has an aggressive phenotype that requires prompt intervention (2). For metastatic disease, the initial medical treatment is androgen deprivation, which induces tumor regression and reduction in serum prostate-specific antigen in 80% to 85% of cases. Unfortunately, androgen-independent tumor recurrence is almost ubiquitous, for which only palliative treatment is available, and even the newest docetaxel-based regimes confer only a 2.4-month survival advantage (3). Death from prostate cancer is the result of metastatic spread, characteristically to the bones, lungs, liver, pleura, and adrenals (4). Bony metastasis is characterized by severe chronic pain, spinal cord compression, and pathologic fractures. Prostate cancer is therefore a highly desirable target for effective and tolerable antimetastatic drugs.

Certain dietary agents may have a preventive effect for prostate cancer, including tomato-derived lycopene, vitamin E, and selenium (5). Furthermore, epidemiologic evidence supports a protective role for high garlic consumption, with one study indicating that high garlic consumption (>10 g/d) was related to low prostate cancer prevalence in China (relative risk, 0.51; $P < 0.001$; ref. 6). Garlic contains a variety of unique organosulfur compounds that have been shown in multiple studies to prevent carcinogen-induced tumorigenesis in laboratory animals, including prostate cancer (7). Garlic also suppresses experimental tumor growth: garlic-fed mice bearing Ehrlich ascites tumors had significantly prolonged survival compared with control (8), and three groups have noted that both s.c. and oral fresh garlic and aged garlic extract (AGE) administration suppressed the growth of transitional cell carcinoma xenografts (9–11). Recently, AGE has also been shown to suppress carcinogenesis in rodent models of hepatocellular and colonic carcinomas (12, 13), and in human clinical trials, 12 months of 2.4 g/d AGE treatment suppressed the formation of colonic adenomas in a sample of 57 patients ($P = 0.04$; ref. 14).

AGE is a widely used dietary supplement obtained from raw garlic by ethanol aging and aqueous extraction. It is more

Authors' Affiliation: Cancer Biology Group, Department of Anatomy, Faculty of Medicine, University of Hong Kong, Hong Kong

Received 8/22/06; revised 11/3/06; accepted 11/15/06.

Grant support: American Institute for Cancer Research (X.Wang).

The costs of publication of this article were defrayed in part by the payment of page charges. This article must therefore be hereby marked *advertisement* in accordance with 18 U.S.C. Section 1734 solely to indicate this fact.

Requests for reprints: Xianghong Wang, Department of Anatomy, The University of Hong Kong, 1/F, Faculty of Medicine Building, 21 Sassoon Road, Hong Kong. Phone: 852-2819-2867; Fax: 852-2817-0857; E-mail: xhwang@hkucc.hku.hk.

doi:10.1158/1078-0432.CCR-06-2074

consistent than fresh garlic in its concentration of stable orally bioavailable organosulfur compounds, including *S*-allylmercaptocysteine (15). Although not present in raw garlic, *S*-allylmercaptocysteine is a major *in vivo* metabolic product of garlic compounds allicin and diallyl disulfide (16), both of which have well-described anticancer properties (7). That the chemical instability of these compounds does not limit their efficacy has led to the suggestion that *S*-allylmercaptocysteine may actually be the bioactive metabolite in both fresh garlic and AGE (17). In fact, *S*-allylmercaptocysteine has been shown to suppress *in vitro* proliferation of cancer cells by mechanisms including apoptosis promotion by c-Jun NH_2-terminal kinase 1 and caspase-3 activation (17) and G_2-M phase cell cycle arrest via direct microtubule disruption (18). Moreover, in prostate cancer cells, *S*-allylmercaptocysteine suppressed proliferation by the additional mechanisms of suppressing prostate-specific antigen production and testosterone levels (19) and altering levels of polyamines and glutathione (20).

Recent *in vitro* studies provide compelling evidence for the potential antimetastatic activity of *S*-allylmercaptocysteine. Without eliciting a mechanism, Hu et al. showed in a novel study that rat sarcoma cell migration was inhibited upon exposure to AGE (21). Indeed, evidence from our laboratory revealed that *S*-allylmercaptocysteine had a potent anti-invasive effect on androgen-independent prostate cancer cells: reducing Matrigel invasion, increasing expression of cell adhesion molecule E-cadherin, and inducing a morphologic change reminiscent of mesenchymal-epithelial transition (22). E-cadherin expression is frequently suppressed in advanced prostate cancer and is a strong independent prognostic indicator of disease progression (23). Its down-regulation is characteristic of the epithelial-mesenchymal transition, a key early step in the metastatic cascade (24). The up-regulation of E-cadherin and reduction in invasiveness by *S*-allylmercaptocysteine is therefore potentially an efficacious method of suppressing tumor progression and metastasis.

Despite the abundant *in vitro* evidence, neither the anticancer effect of *S*-allylmercaptocysteine nor the antimetastatic ability of any garlic compound has been reported on *in vivo*. This study was therefore designed to study the *in vivo* effect of *S*-allylmercaptocysteine on prostate cancer growth, metastatic ability, and toxicity. To achieve this, we developed a fluorescent orthotopic severe combined immunodeficient (SCID) mouse model of androgen-independent prostate cancer and examined the effects of *S*-allylmercaptocysteine treatment on tumor growth and spread. Our results provide the first evidence that *S*-allylmercaptocysteine suppresses both the growth and distant metastasis of advanced androgen-independent prostate cancer xenografts *in vivo* without inducing organ pathology or other signs of manifest toxicity. *S*-allylmercaptocysteine is therefore a highly promising novel candidate for inclusion in clinical trials as an antimetastatic drug for androgen-independent prostate cancer patients.

Materials and Methods

S-allylmercapto-L-cysteine. *S*-allylmercaptocysteine (purity >95%) was a generous gift from Wakunaga Pharmaceutical Co. Ltd. (Hiroshima, Japan). It was fed to mice as an acidified (pH 4.5) suspension of 30 mg/mL in 10% (w/v) L-dextrose, 1% (w/v) gum arabic (Sigma-Aldrich, St. Louis, MO).

Parental PC-3 and green fluorescent protein–expressing PC-3 cell line. PC-3 cells were obtained from the American Type Culture Collection (Manassas, VA) and cultured in RPMI 1640 supplemented with 5% (w/v) FCS and 1% (w/v) penicillin-streptomycin (Invitrogen, Carlsbad, CA). An expressing vector containing green fluorescent protein (GFP) sequence was constructed using Virapower Lentiviral gene expression system according to the manufacturers' instructions (Invitrogen). Briefly, GFP cDNA was amplified from the pEGFP empty vector by PCR and was then cloned into the plenti6/V5-D-Topo vector (Invitrogen). This construct was transfected into the Lentiviral packaging cell line 293FT together with ViraPower packaging mix (Invitrogen) using Fugene 6 transfection reagent (Roche Diagnostics, Indianapolis, IN). Virus-containing culture medium was collected after 48 h and filtered through a 0.45-μm syringe filter. The viruses were mixed with 6 μg/mL polybrene (Sigma-Aldrich) and used to infect PC-3 cells by adding directly into the culture medium. Forty-eight hours after infection, the cells were exposed to 8 μg/mL blasticidin for 6 days, and GFP-expressing clones were visualized by microscopy before transfer using the clonal ring. We generated six clones of stable, high-level GFP-expressing cells from which we selected the clone PC-3 GFPC3 (PC-3 GFP-expressing clone 3) due to its phenotypic similarity to the parental PC-3 cell line.

Western blotting. Previously described technique was used (25). Briefly, we prepared total cell lysate by cell scraping using radioimmunoprecipitation assay lysis buffer [150 mmol/L NaCl, 50 mmol/L Tris/HCl (pH 8), 1% (w/v) NP40, 0.5% (w/v) deoxycholate, 0.1% (w/v) SDS plus protease inhibitors, 1 mmol/L phenylmethylsulfonyl fluoride, 1 μg/mL aprotinin, 1 μg/mL leupeptin] followed by 15 min of centrifugation at 14,000 rpm, 4°C to remove cellular debris. Protein concentration was calculated using DC Protein Assay kit (Bio-Rad, Hercules, CA). Equal amounts of 30 μg protein were loaded into each well of 10% (w/v) polyacrylamide gels for electrophoresis followed by transfer onto a polyvinylidene difluoride membrane (Amersham, Piscataway, NJ). Membranes were blocked overnight at 4°C in 10% (w/v) nonfat milk and incubated for 1 h at room temperature with primary antibodies: E-cadherin, actin, and GFP (BD Biosciences, San Jose, CA; Santa Cruz Biotechnology, Santa Cruz, CA; and Roche, Mannheim, Germany, respectively). Signals were transduced with the appropriate horseradish peroxidase–conjugated secondary antibody and detected using the enhanced chemiluminescence Western blotting system (Amersham).

Bromodeoxyuridine incorporation assay. Previously described technique was used (25). Cells were grown onto coverslips for 24 h until ~60% confluent and treated for 1 h with 10 μmol/L bromodeoxyuridine (Sigma-Aldrich). The cells were then fixed in ice-cold 70% ethanol for 30 min. Coverslips were washed in cold PBS, incubated in 2 mol/L HCl for 20 min, and neutralized in 0.1 mol/L borate buffer (pH 8.5). The slides were then blocked with 0.1% bovine serum albumin in PBS before incubation with anti-bromodeoxyuridine antibody (Roche). After rinsing, rhodamine-conjugated goat anti-mouse IgG secondary antibody was added for 1 h, and the cells were then counterstained with 4′,6-diamidino-2-phenylindole. At least 500 cells were counted from four randomly selected fields per slide, and percentage of bromodeoxyuridine-positive cells was calculated. The experiment was reproduced at least four times.

Orthotopic tumor implantation. Previously described operative technique was applied (26). Briefly, 6- to 8-week-old CB-17 SCID/SCID mice were held according to the Guide for the Care and Use of Laboratory Animals, University of Hong Kong. Under surgical access, 10^6 cells in 20 μL serum-free RMPI 1640 were injected into the dorsal prostate using a glass syringe with 30-gauge needle (Hamilton, Reno, NV). Organs were then replaced, and the abdomen was closed in two layers with 5-0 silk suture. The animals commenced treatment on day 4 of control (vehicle, $n = 6$), 100 mg/kg (low dose) *S*-allylmercaptocysteine ($n = 5$), and 300 mg/kg (high dose) *S*-allylmercaptocysteine ($n = 6$) by daily orogastric feeding. After 28 days of treatment, the mice were euthanized by cervical dislocation and meticulously examined at postmortem (magnification, ×10).

Tissue processing. To obtain toxicity data, a control mouse and one mouse treated with 300 mg/kg/d *S*-allylmercaptocysteine for 28 days were euthanized, and their livers, kidneys, and stomach were placed in 10% neutral buffered formalin for 24 h before dehydration in graded alcohol and embedding in paraffin. Sections were cut at 4-μm thickness in at least five separate areas of each organ, processed, and carefully compared with control. H&E staining and immunohistochemical study were done; the latter using anti-human cytokeratin 18 IgG antibody (Santa Cruz Biotechnology). To generate frozen sections, formalin-fixed organs were transferred to 30% (w/v) sucrose solution in 0.1 mol/L sodium dihydrogen phosphate buffer (pH 7.3) for 48 h and were then frozen at −80°C before sectioning.

Blood samples. Blood samples (100 μL) were drawn immediately before euthanasia by left ventricular puncture and incubated in 400 μL ice-cold ammonium chloride red cell lysis buffer [0.15 mol/L NH_4Cl/0.2 mol/L Tris-HCl (pH 7.2)] for 4 min at 4°C. The lysis was stopped by addition of 2 mL sterile ice-cold PBS and centrifugation at 2,000 rpm for 2 min. The pellet was resuspended in 4 mL RPMI 1640 and incubated at 37°C for 24 h in a 50-mm Petri dish (Iwaki, Tokyo, Japan). For cell spiking experiments, 50 μL of blood was mixed with 10 μL PBS containing 10, 50, and 100 cells. This experiment was repeated in triplicate.

Fluorescent microscopy. The cells and slides were exposed to a mercury lamp at 480-nm wavelength, and GFP emission was captured at 520 nm using a Leica DM IRB microscope. Images were captured using the Advanced Spot System software and a Chinetek 2e Enhanced camera. For identification of primary tumor and lymph node metastases, five 50-μm-thick sections were cut from each sample at least 200 μm apart Solid organs, lung, and adrenal were submitted to serial 40-μm section and screened under ×40 magnification microscopy for green fluorescent deposits. Positive signals were confirmed to contain tumor cells by higher power examination (×100) before being designated metastases. Blood samples were viewed in 50-mm culture Petri dishes and were meticulously scanned for presence of viable fluorescing tumor cells.

Statistical analysis. The results were analyzed by SPSS 14.0 (Aspire Software International, Leesburg, VA). The data from each experiment were compared by either ANOVA or Mann-Whitney *U* test, depending on the mode of distribution. *P*s were deemed significant when $P < 0.05$. All statistics are presented in text and figures as mean ± SE.

Results

The green fluorescent cell line PC-3 GFPC3 was phenotypically unchanged in comparison to parental PC-3 cells. To enable direct visualization of metastatic lesions in the mouse, we engineered the androgen-independent metastatic prostate cancer cell line PC-3 to constitutively express GFP using stable retroviral transfection techniques. One clone (PC-3 GFPC3) was shown by Western blot (Fig. 1A) and microscopy (Fig. 1B) to have universal expression of GFP protein, whereas the parental PC-3 (control) was negative for fluorescence and GFP expression. Bromodeoxyuridine incorporation assay confirmed that there was no significant alteration in PC-3 GFPC3 cell proliferation rate compared with parental cells ($P = 0.42$; Fig. 1C). We then used Western blot to show that the expression of GFP was not altered in the cells in response to treatment with *S*-allylmercaptocysteine, whereas the previously described dose-dependent up-regulation of E-cadherin persisted (Fig. 1D; ref. 22). These results were suggestive of successful generation of a stable GFP-expressing PC-3 cell line with equivalent properties to the parental cells.

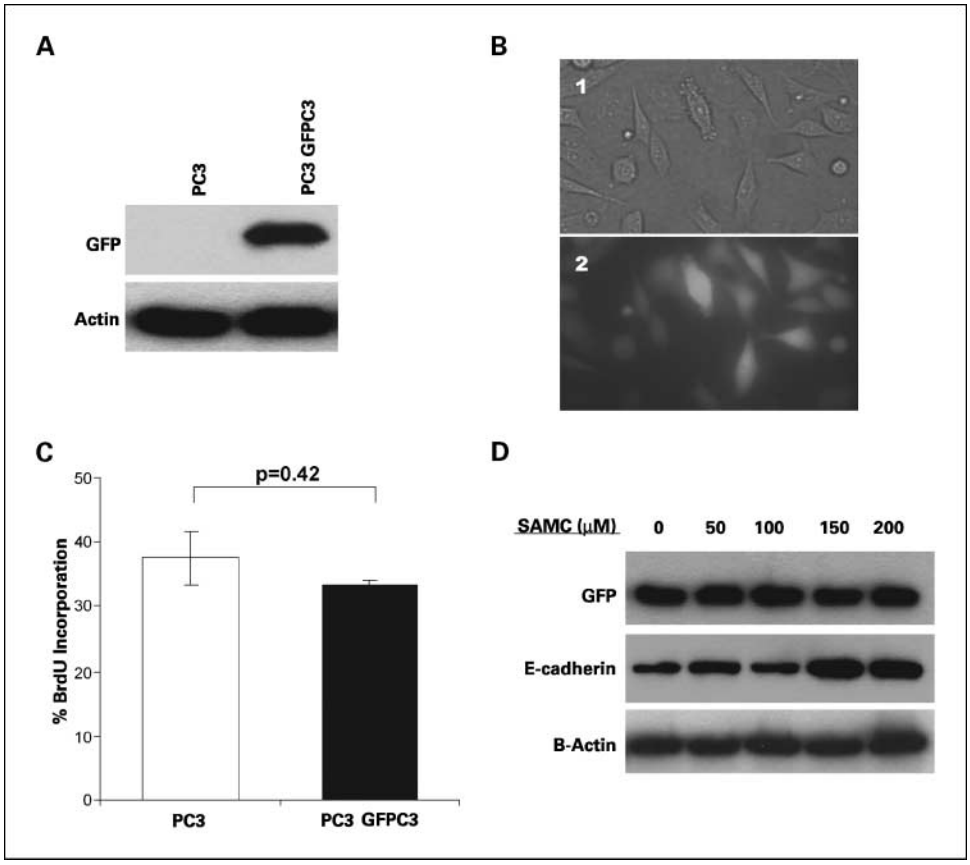

Fig. 1. The generation and characterization of fluorescent PC-3 GFPC3 cells. *A,* GFP-transfected but not parental cells show expression of high levels of GFP protein by Western blotting. *B,* ×100 images of transfected PC-3 GFPC3 cells under inverted light field and fluorescent microscopes. Note that these cells ubiquitously fluoresce bright green under the fluorescent microscope. *C,* bromodeoxyuridine (*BrdU*) incorporation rate in parental and GFP-transfected cells. Bromodeoxyuridine incorporation assay shows no significant difference in proliferative index ($P = 0.42$). *D,* expression of GFP and E-cadherin after exposure to different doses of *S*-allylmercaptocysteine (*SAMC*) by Western blotting. Note that *S*-allylmercaptocysteine has no notable effect on the expression of GFP but significantly increases expression of E-cadherin.

PC-3 GFPC3 cells formed metastatic GFP-expressing tumors in SCID mice. By injecting 10^6 PC-3 GFPC3 cells into the dorsal prostate of four SCID mice, we showed that our method of surgical orthotopic implantation induced not only primary tumor formation (Fig. 2A, *1*, *circled area*) but also lymph node metastases (Fig. 2A, *2*, *circled area*) in 100% of animals after 30 days. All positive lymph nodes from each group were located in the loco-regional drainage area, with no identifiable lymph node spread across the diaphragm or into the limbs. H&E sections of the primary tumors (Fig. 2B, *1*) and lymph nodes (Fig. 2B, *2*) revealed large undifferentiated cells with prominent and irregular nuclei, consistent with tumor cell origin. We then used human cytokeratin-18 immunohistochemistry on the lymph node sections and verified that these tumor cells were of human origin (Fig. 2C). At subsequent fluorescent microscopy, all areas of tumor formation displayed bright green fluorescence, confirming the PC-3 GFPC3–derived origin of the primary (Fig. 2D, *1*) and lymph node deposits (Fig. 2D, *2*). Green fluorescent tumor deposits were subsequently identified in the lungs of 100% of the mice (representative image is shown in Fig. 2E, counterstained with 4′,6-diamidino-2-phenylindole). Additionally, deposits were identified in the adrenals of 75% of the mice, but no liver or kidney metastases were observed. These results indicated the successful establishment of an androgen-independent prostate cancer orthotopic model, which would enable high-sensitivity detection of metastases in the lungs and adrenals.

S-allylmercaptocysteine did not provoke any macroscopic or histologic organ pathology at a dose of 300 mg/kg/d. To exclude

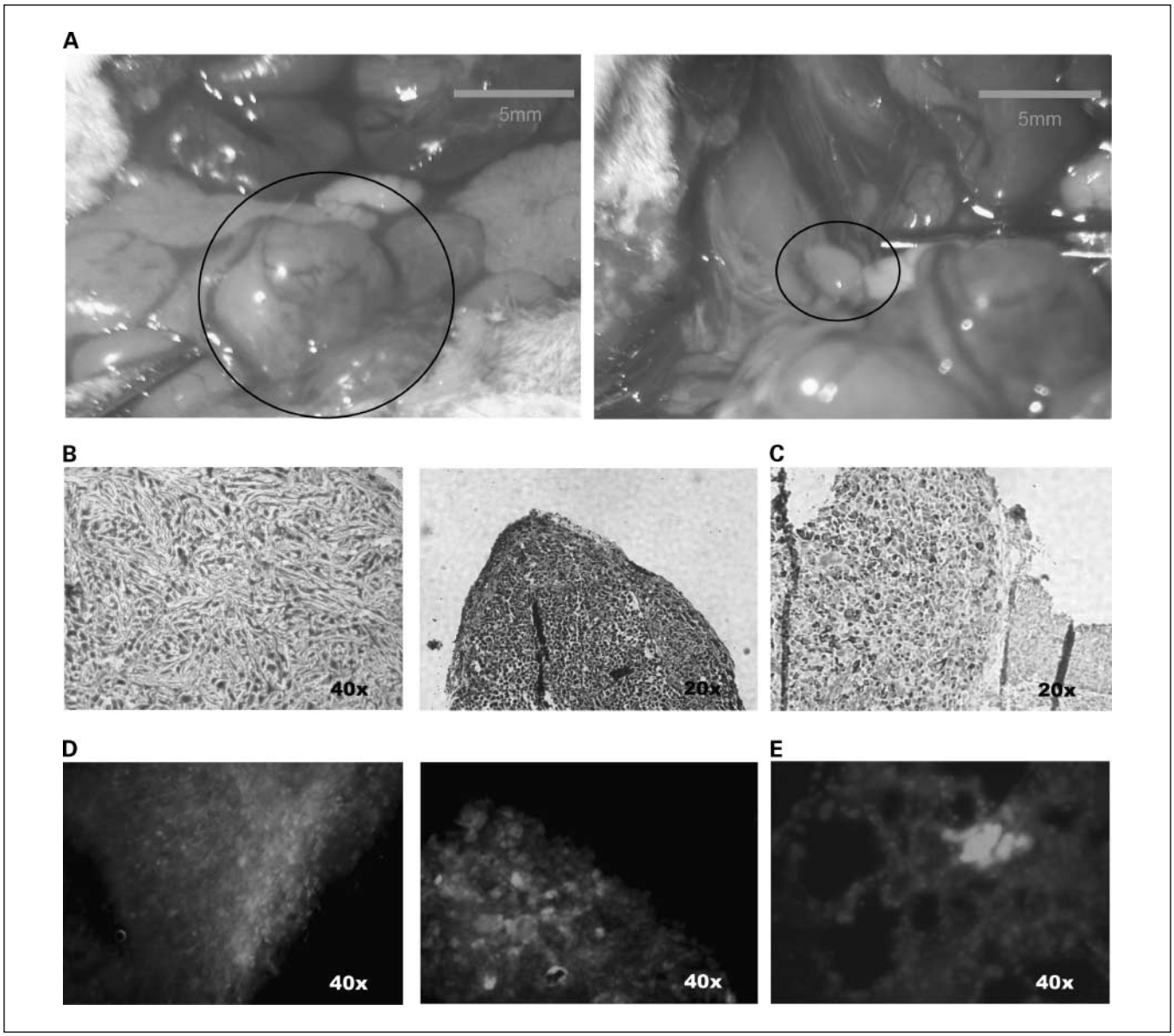

Fig. 2. The fluorescent orthotopic model of prostate cancer produces reliable and easily identifiable metastatic disease. *A,* macroscopic view of primary tumor (*left, circled*) and lymph node metastasis (*right, circled*) at postmortem. Magnification, ×4. *B,* H&E sections of primary and lymph node showing the presence of morphologically undifferentiated tumor cells in both primary tumor (*left*) and lymph node (*right*). *C,* a section of lymph node stained for human cytokeratin-18 using immunohistochemistry. *D,* fluorescent images of primary tumor (*left*) and lymph node metastasis (*right*) showing clear and ubiquitous fluorescence. *E,* fluorescent image of lung metastasis. This frozen section was counterstained with 4′,6-diamidino-2-phenylindole and shows a multicellular green fluorescent metastasis in the lung periphery.

serious toxicity, we screened for the presence of organ pathology in *S*-allylmercaptocysteine–treated mice using a 50% higher dose (300 mg/kg/d) than the maximum previously described (27). After treating for 30 days, no anatomic abnormalities or signs of inflammation, necrosis, or hemorrhage were observed at postmortem evaluations. In addition, H&E sections of the liver (Fig. 3A, *1a* and *1b*), kidney (Fig. 3A, *2a* *2a* and *2b*), and stomach (Fig. 3A, *3a* and *3b*) revealed normal tissue architecture and cellular morphology in both control (*top a*) and treated (*bottom b*) animals. Our initial investigations, therefore, did not provide any evidence of toxicity for up to 300 mg/kg/d *S*-allylmercaptocysteine.

S-allylmercaptocysteine treatment did not provoke any clinical signs of toxicity or loss of weight at doses of up to 300 mg/kg/d. To investigate the tumor-suppressive effects of *S*-allylmercaptocysteine on our mouse model of androgen-independent prostate cancer, we injected 10^6 PC-3 GFPC3 cells into the dorsal prostate of 17 SCID mice. Three days after injection, the mice were randomized into three groups: control ($n = 6$), low-dose (100 mg/kg/d) *S*-allylmercaptocysteine ($n = 5$), and high-dose (300 mg/kg/d) *S*-allylmercaptocysteine ($n = 6$). To assess the toxicity of *S*-allylmercaptocysteine, we monitored the response of mouse body weight to treatment as a percentage of starting weight (Fig. 3B). Having found no significant difference between the starting mean mouse weights in each group ($P > 0.8$), we did not observe any weight alteration in any treatment group by the end point. In fact, the control group (*solid line*) showed a trend towards decreasing body mass over the final 3 days, potentially due to high tumor burden, although this did not reach significance when compared with the low-dose or high-dose treated groups (*dotted line*; $P = 0.08$). These results, together with the organ histology data (Fig. 3A), indicate that chronic administration of up to 300 S-allylmercaptocysteine is tolerable in mice.

S-allylmercaptocysteine suppressed the growth of primary orthotopic PC-3 tumors in SCID mice in a dose-dependent manner. To study the effect of *S*-allylmercaptocysteine administration on primary tumor growth, we euthanized the mice after 28 days treatment and excised and weighed the primary tumors. Control and low-dose *S*-allylmercaptocysteine–treated mice universally yielded relatively large palpable primary tumors (Fig. 3C, *1* and *2*), whereas those from 300 mg/kg/d *S*-allylmercaptocysteine–treated mice were visibly smaller (Fig. 3C, *3*), including one microscopic primary tumor that was too small to identify at postmortem (Fig. 3C, *4*, *arrow*). Frozen sections of tumor specimens were found to fluoresce strongly and did not contain significant amounts of nonfluorescing (mouse) tissue. Data analysis revealed that high-dose *S*-allylmercaptocysteine induced a mean 71% suppression of tumor mass compared with control ($P < 0.001$; Fig. 3D). Low-dose *S*-allylmercaptocysteine, however, did not induce significant tumor shrinkage ($P = 0.09$), and high-dose *S*-allylmercaptocysteine was significantly more effective than low dose ($P = 0.027$). These data show that *S*-allylmercaptocysteine at 300 mg/kg/d is able to suppress the growth of androgen-independent prostate tumors *in vivo*.

***S-allylmercaptocysteine treatment suppressed the formation of distant prostate cancer metastases* in vivo.** Loco-regional lymph node metastasis is a frequent early stage in tumor progression; thus, we resected, counted, and weighed the visible lymph nodes from each mouse. Unexpectedly, we did not find any significant decrease in the number or weight of metastatic lymph nodes in either high-dose or low-dose *S*-allylmercaptocysteine treatment (Fig. 4A). The presence of distant metastasis is frequently the critical difference between curable and terminal cancer. Therefore, to assess the potential inhibitory effects of *S*-allylmercaptocysteine on distant metastatic spread, we evaluated the entire lungs and adrenals of each mouse for the presence of multicellular metastases. In the lungs, we observed a significant 85.5% reduction ($P = 0.001$) in the mean number of metastases identifiable per mouse following high-dose 300 mg/kg/d *S*-allylmercaptocysteine compared with control (Fig. 4B). Low-dose *S*-allylmercaptocysteine produced a trend to decrease lung metastasis formation, but this did not reach significance compared with control ($P = 0.33$). We next analyzed the adrenals, again finding a clear reduction in number of metastases following treatment. In fact, 300 mg/kg/d *S*-allylmercaptocysteine completely abolished the presence of metastases ($P = 0.02$; Fig. 4C). These results revealed that *S*-allylmercaptocysteine therapy significantly reduces distant metastasis to multiple distant organ sites in a dose-dependent manner.

S-allylmercaptocysteine treatment significantly reduced the number of circulating tumor cells. In light of our observation that *S*-allylmercaptocysteine is able to suppress the formation of distant metastasis, we isolated and quantified the number of viable (fluorescing) tumor cells in the circulation to assess whether or not *S*-allylmercaptocysteine could reduce their presence. We used partial red cell lysis followed by nucleated cell extraction, culture, and fluorescent microscopy to quantify circulating tumor cell (CTC) number (representative images shown in Fig. 5A). To assess the efficacy of this method, we used cell spiking experiments to study the relationship between known numbers of viable cells added to blood and number of cells subsequently detected in culture. We established a linear input detection relationship with high-recognition efficiency (mean, 78.5%; Fig. 5B), which supported the quantitative accuracy of our CTC isolation method. We then used this method to quantify CTCs in the blood of our experimental mice. By sampling 100 μL of arterial blood from each mouse immediately before euthanasia, we discovered that high-dose *S*-allylmercaptocysteine treatment reduced the mean number of CTCs by 91% compared with control ($P = 0.041$; Fig. 5C). Additionally, the number of mice with detectable CTCs was decreased from 83.3% of mice in the control group to 40% in the low dose–treated group and 16.6% in the high dose–treated group. These results suggest that the *S*-allylmercaptocysteine treatment may inhibit the invasive step in which primary tumor cells detach and intravasate or may reduce the survival of tumor cells in the circulation.

Discussion

In this study, using an orthotopic SCID mouse model of advanced androgen-independent prostate cancer, we provide the first evidence that aged garlic–derived compound *S*-allylmercaptocysteine can inhibit the growth and progression of prostate cancer xenografts *in vivo*. Our results showed that *S*-allylmercaptocysteine is able to suppress distant metastasis to the lungs and adrenals without inducing overt toxicity, indicating that *S*-allylmercaptocysteine may be a novel and

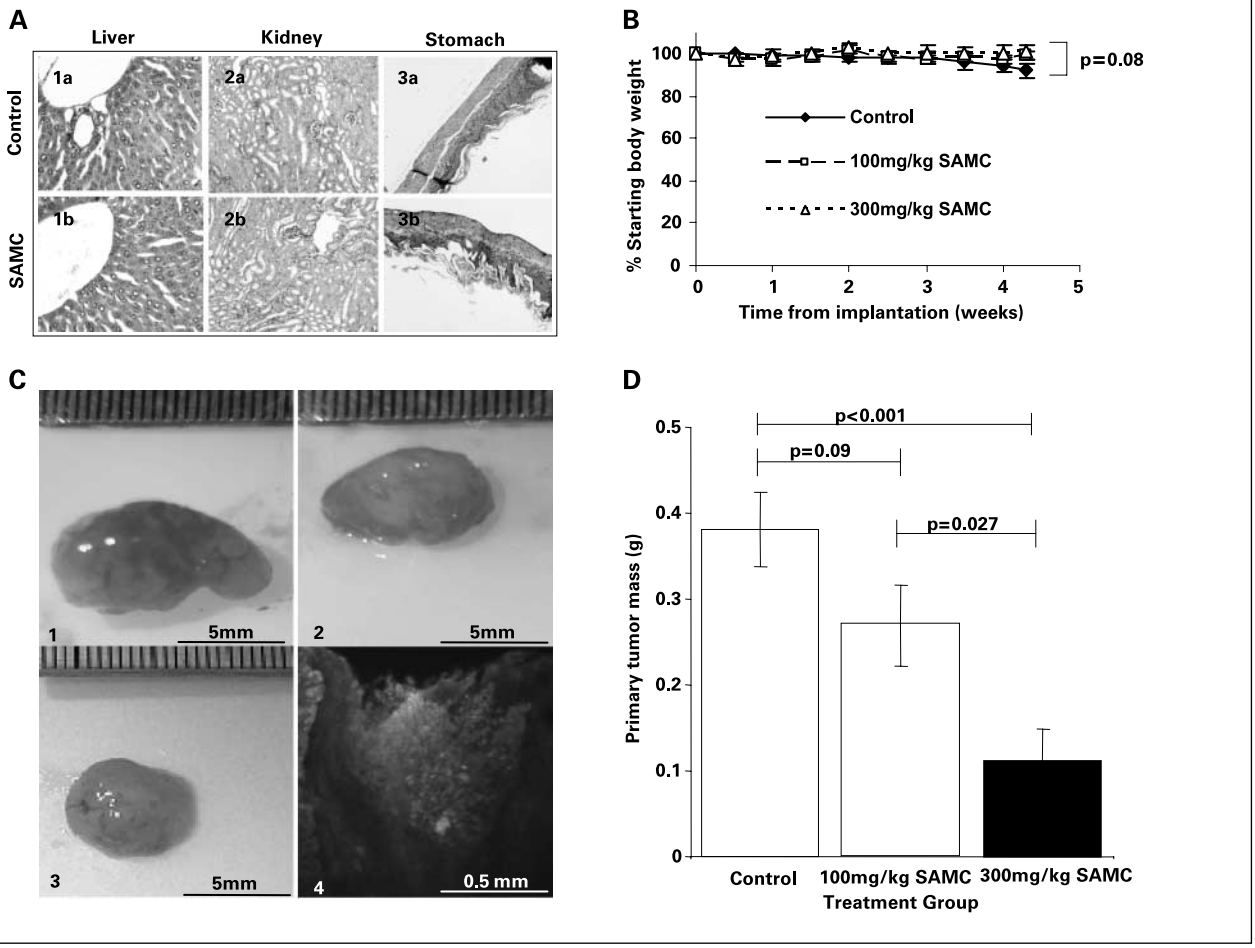

Fig. 3. *S*-allylmercaptocysteine inhibits the growth of primary tumors without notable evidence of toxicity. *A,* H&E sections of liver (*1*), kidney (*2*), and stomach (*3*) from control (*a*) and high-dose *S*-allylmercaptocysteine – treated mice (*b*). Sections show no structural pathology in any organ in either group, supporting the low toxicity of *S*-allylmercaptocysteine treatment. *B,* serial weight measurements of the experimental mice. Weight was normalized to 100% of original at day 1. Note the absence of significant decrease in body weight at any stage in control, low-dose treatment, or high-dose treatment, despite a trend towards decreasing body weight in control mice after week 4 ($P = 0.08$). *C,* representative images of the macroscopic appearance of resected primary tumors after 28 days treatment. Tumors shown are the median tumors treated with vehicle (*1*), 100 mg/kg/d *S*-allylmercaptocysteine (*2*), and 300 mg/kg/d *S*-allylmercaptocysteine (*3*). Frozen section of a microscopic primary (*4*) from the high-dose *S*-allylmercaptocysteine group that was not visible at postmortem. *D,* quantitative analysis of primary tumor mass. Note that 300 mg/kg/d *S*-allylmercaptocysteine treatment induced a significant decrease in mean primary tumor size ($P < 0.001$).

effective antimetastatic treatment in androgen-independent prostate cancer.

Orthotopic models of cancer have been shown to be a powerful tool for studying anticancer drug efficacy because they reproduce the microenvironment and circulation of primary tumors in humans (28). Similar to previous studies, our prostate cancer model produced multicellular metastases to the lymph nodes and lungs in 100% of mice within 30 days (26). Furthermore, the sites of metastatic involvement in our model are highly representative of terminal human prostate cancer (4), with the notable exception of bony metastasis, which is notoriously hard to recreate in laboratory animals (29). The use of GFP-expressing cells for orthotopic implantation is a recently developed approach that significantly improves the efficiency of metastasis identification by permitting direct and unambiguous detection (Fig. 2; ref. 26). Although similar fluorescent orthotopic prostate cancer models have been used to test experimental drug efficacy in at least two other studies (30, 31), in this study, we used high-power microscopy on serial frozen tissue sections instead of counting organ surface lesions at fluorescence-assisted dissection, which may not distinguish deeply located organ metastases (32). As evidence supporting our methodology, the mean number of metastases we identify per control mouse is greater (6.5 per mouse) than that described by Pchejetski et al. (3.4 per mouse) using the same 30-day end point (31). This suggests higher detection efficiency in our model, although direct comparison was not done.

Using this SCID mouse model, we showed for the first time that *S*-allylmercaptocysteine suppresses primary PC-3 cell androgen-resistant prostate tumor growth *in vivo*. As we have discussed above, *S*-allylmercaptocysteine induces cancer cell death through multiple pathways (17–20). Our results suggest that these previous *in vitro* data translate into successful tumor growth suppression *in vivo*. Unfortunately, many compounds that suppress tumor xenograft growth in preclinical models are later found to induce unacceptable toxicity in humans at effective doses, indicating the necessity for toxicity surveillance in experimental animals. At the effective dose of 300 mg/kg/d

S-allylmercaptocysteine, however, not only did we observe maintenance of healthy body weight and absence of clinical manifestations of toxicity, but we also found no evidence of morphologic pathology in organs susceptible to *S*-allylmercaptocysteine–induced damage (Fig. 3A and B). Specifically, we studied liver and kidney because garlic compounds undergo hepatic metabolism and are excreted in the urine (15), and we assessed the stomach epithelium due to its direct exposure to concentrated *S*-allylmercaptocysteine. In fact, previous animal studies showed that 200 mg/kg *S*-allylmercaptocysteine actually protected against toxin-induced liver damage, with similar efficacy to human hepatoprotective drug *N*-acetylcysteine (27). It is noteworthy that *N*-acetylcysteine has a similar cysteine-based chemical structure to *S*-allylmercaptocysteine and is administered routinely to humans in oral doses of 540 mg/kg/d, supporting the clinical relevance of the 300 mg/kg/d *S*-allylmercaptocysteine dose we administered to our mice. Additionally, *S*-allylmercaptocysteine exposure preexists in humans through dietary consumption of fresh garlic and AGE, which has been administered to humans under controlled conditions in doses as high as 10 g/d without severe adverse effects (15). Therefore, whereas formal human toxicity studies will be necessary to permit its clinical use, low-dose exposure to *S*-allylmercaptocysteine is already prevalent, and our preclinical evidence indicates that it has tolerable toxicity in effective anticancer doses in mice.

Despite these findings, we surprisingly did not observe a significant alteration in the size or quantity of lymph node metastases following treatment with *S*-allylmercaptocysteine. One explanation for this phenomenon may be that the injection of individual cells into the prostate parenchyma provides direct access to the lymphatic system and predisposes to immediate loco-regional node involvement, which we are in the process of modifying for future studies. Nonetheless, the ability of *S*-allylmercaptocysteine to suppress distant metastasis is the crucial factor in reducing clinical morbidity and mortality (33), and persistence of noninvasive lymph node disease should not represent a significant obstacle to its clinical

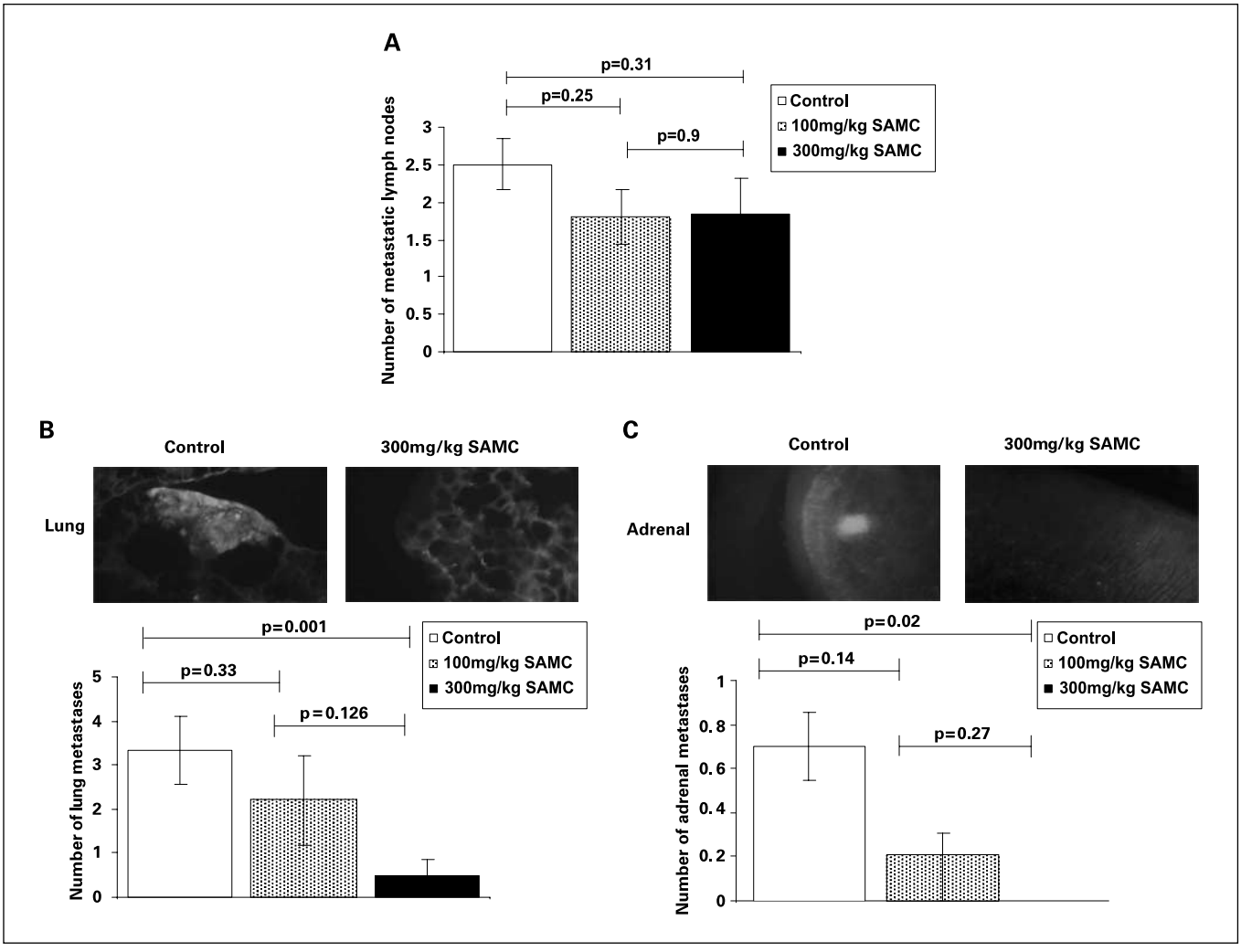

Fig. 4. High-dose *S*-allylmercaptocysteine treatment inhibits the formation of distant metastases. *A,* quantitative analysis of number of positive lymph nodes. Note that we identified no significant decrease in number of lymph node metastases following treatment at either dose. *B* and *C,* frozen sections of the lungs (*B*) and adrenals (*C*) from control and *S*-allylmercaptocysteine–treated mice were examined for positive green fluorescent signals with a fluorescent microscope under ×40 magnification. Representative images and quantitative analysis. *B,* note that *S*-allylmercaptocysteine treatment suppresses the formation of lung metastases in a dose-dependent manner by up to 85% in high-dose group ($P = 0.001$). *C,* note that *S*-allylmercaptocysteine completely abolished the presence of adrenal metastases in high dose–treated group ($P = 0.02$).

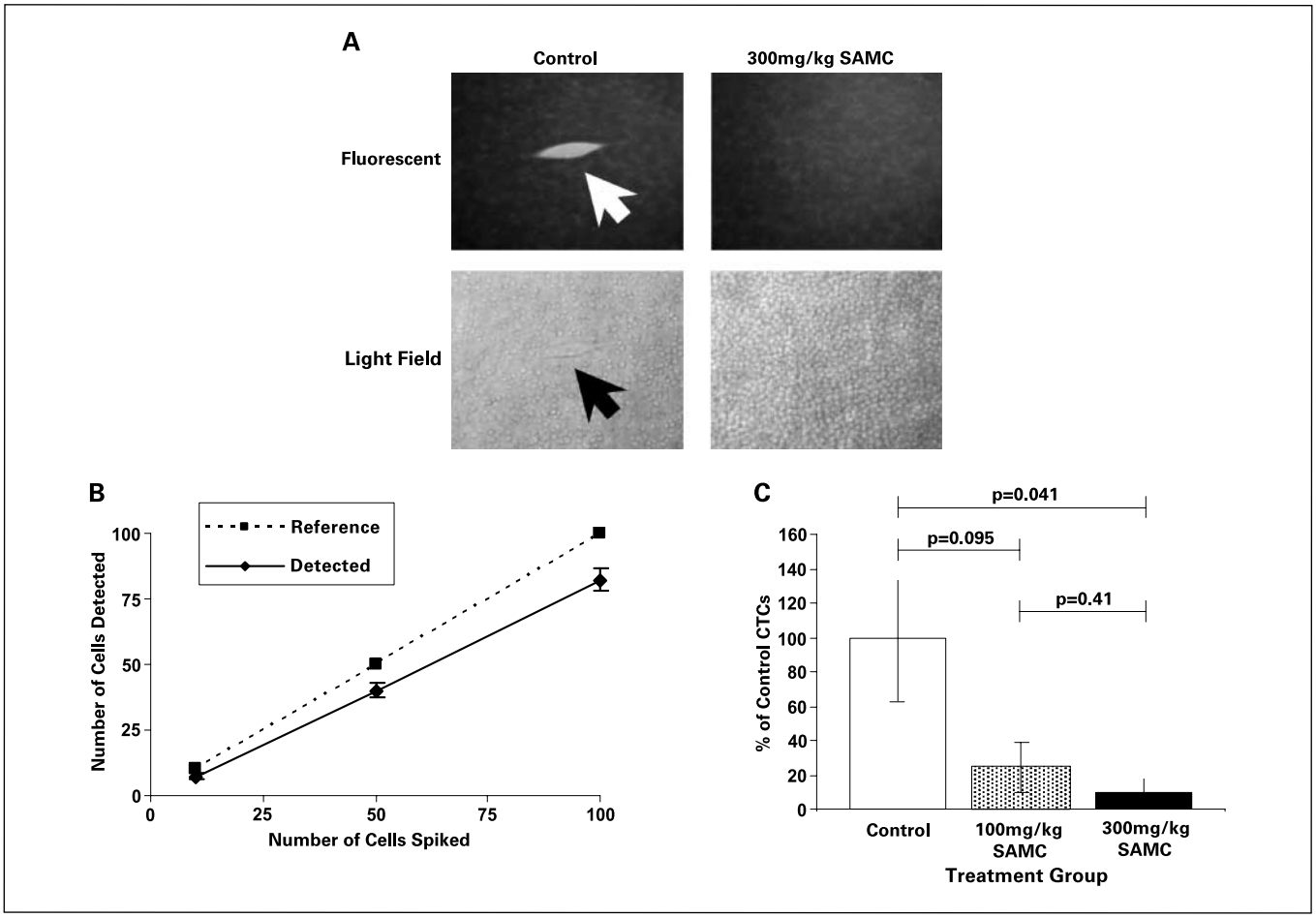

Fig. 5. *S*-allylmercaptocysteine treatment reduces the presence of circulating tumor cells. *A,* representative image of CTCs isolated from mice and held in culture visualized by inverted and fluorescent microscopy under ×100 magnification. Left, attached, fluorescing (*top*) PC-3 GFPC3 cell isolated from the circulation of a control mouse. The cell is surrounded by some remaining erythrocytes from incomplete red cell lysis (inverted light microscope, *bottom*). Right, absence of fluorescent cells as seen in five of six high-dose *S*-allylmercaptocysteine – treated mice. *B,* graphic representation of the efficiency and accuracy of our viable CTC detection method. The graph displays the number of cells spiked into each blood sample on the *x*-axis (*dotted line*) compared with the number of cells observed at fluorescent microscopy the following day (*solid line*). *C,* relative numbers of CTCs in the blood of the *S*-allylmercaptocysteine – treated mice (*filled columns*) compared with the control (indicated as 100%; *open column*).

application. In fact, tumor dissemination and metastasis is frequently fatal and is the main obstacle to successful cancer treatment. In this study, we revealed that high-dose *S*-allylmercaptocysteine therapy reduced the number of lung metastases by 85% and completely abolished the presence of adrenal metastases, representing a considerable clinical advantage over control-treated mice (Fig. 4B and C). Previous studies from our laboratory have shown that *S*-allylmercaptocysteine reduces migration and invasion of androgen-independent prostate cancer cells via an up-regulation of E-cadherin (22), which we also observed in PC-3 GFPC3 cells (Fig. 1D). E-cadherin is the functional unit of the adherens junction, and loss of functional E-cadherin increases cell motility, which is consistently linked with cancer progression due to disruption of epithelial integrity. In previous studies, exogenous overexpression of E-cadherin in cholangiocarcinoma cells not only promoted cell-cell adhesion but also decreased cell proliferation, motility, and invasion (34). Additionally, E-cadherin up-regulating agent 5-aza-2′-deoxycytidine was able to suppress metastases in a metastatic mouse model of breast cancer (35). Consistent with the previously E-cadherin – dependent described anti-invasive mechanism of *S*-allylmercaptocysteine (22), these studies therefore indicate that restoring E-cadherin expression is an effective mechanism of reducing tumor invasion and metastasis *in vivo*. This supports our data that show that the *in vitro* anti-invasive properties of *S*-allylmercaptocysteine translate into effective metastasis suppression *in vivo*.

Metastasis to distant solid organs, such as the lungs and the adrenals, is conditional on the delivery of tumor cells via the bloodstream, and previous studies have shown that viable PC-3 cells are present in the bloodstream of orthotopically implanted mice and can be identified by their fluorescence (36). Significantly, abnormality of E-cadherin expression has also been shown to be the strongest independent variable predicting presence of CTCs in the blood in humans ($P < 0.0001$; ref. 37). We therefore isolated and quantified the number of viable tumor cells in the circulation to assess whether or not *S*-allylmercaptocysteine could reduce their presence (representative images are shown in Fig. 5A). Our results showed that *S*-allylmercaptocysteine treatment remarkably reduced the presence and number of viable CTCs by 91% compared with control (Fig. 5). Presence of CTCs has been correlated in a

number of studies with advanced cancer stage and is strongly predictive of poor disease prognosis in prostate, breast, and colon cancers (38). Together with previous evidence, our results suggest that the inhibitory effect of *S*-allylmercaptocysteine on distant metastasis may be the result of its suppressive effect on CTCs, possibly through its negative effect on tumor cell migration and invasion as previously suggested (22). Of additional note, Chu et al. have shown that *S*-allylmercaptocysteine down-regulates *Snail*, the transcriptional repressor of E-cadherin (22). In addition to its regulation of epithelial cell-cell adhesion, Snail stimulates the production of matrix metalloproteinase-2 and matrix metalloproteinase-9, both of which promote tumor cell motility and degrade basement membranes, and are involved in prostate cancer and tumor cell intravasation (39). It is therefore possible that *S*-allylmercaptocysteine–mediated suppression of the Snail signaling pathway may play a role in the reduction in invasion and intravasation; however, this hypothesis requires further study. Regardless of the dominant mechanism involved, we show that *S*-allylmercaptocysteine limits the *in vivo* spread of androgen-independent prostate cancer cells, suggesting a great potential for its clinical application.

In terms of the indications for the use of antimetastatic drugs such as *S*-allylmercaptocysteine, it seems that prostate cancer is particularly well suited due to its frequently long latent stage, complex natural history, and limited response to conventional cytotoxic chemotherapy. The results from our orthotopic PC-3 model indicate a role for *S*-allylmercaptocysteine in treating terminally advanced metastatic androgen-independent prostate cancer. Due to its apparently low toxicity, *S*-allylmercaptocysteine could also be a suitable adjuvant oral drug for high-grade localized disease in elderly men with a short life expectancy or poor tolerance for surgery or cytotoxic therapy. Furthermore, with the advent of widespread prostate-specific antigen screening and the consequently prevalent clinical presentation of low-grade, early-stage tumors, the current use of the "watchful waiting" strategy could be supplemented with oral *S*-allylmercaptocysteine therapy to reduce the incidence of tumor progression. However, it should be noted that PC-3 is a highly undifferentiated cell line that represents an unusually advanced and metastatic form of prostate cancer. Future testing on less aggressive androgen-independent prostate cancer xenograft models, as well as yet-undeveloped spontaneous bone metastatic models, will therefore be required to confirm the prostate specificity of the anticancer and antimetastatic effects of *S*-allylmercaptocysteine. Importantly though, because neither the growth-inhibitory (40) nor the anti-invasive (22) effects of *S*-allylmercaptocysteine seem to be prostate specific, our findings imply that *S*-allylmercaptocysteine may in fact be a universal antimetastatic agent for the treatment of advanced carcinomas.

In summary, we present the first evidence that garlic-derived *S*-allylmercaptocysteine is an effective anticancer drug in a mouse model of advanced prostate cancer. More importantly, we have shown a significant antimetastatic effect of *S*-allylmercaptocysteine against androgen-independent prostate cancer xenografts *in vivo*, possibly through suppression of viable circulating tumor cells. This is the first *in vivo* report of the antimetastatic properties of any garlic compound. It is hoped that our evidence may lead to further studies, including clinical trials on human subjects, to fully explore the potential of *S*-allylmercaptocysteine in the treatment of advanced prostate cancer.

Acknowledgments

We thank Wakunaga Pharmaceutical Co. Ltd. for the supply of *S*-allylmercaptocysteine compound.

References

1. Edwards BK, Brown ML, Wingo PA, et al. Annual report to the nation on the status of cancer, 1975-2002, featuring population-based trends in cancer treatment. J Natl Cancer Inst 2005;97:1407–27.
2. Bracarda S, de CO, Greco C, et al. Cancer of the prostate. Crit Rev Oncol Hematol 2005;56:379–96.
3. Tannock IF, de WR, Berry WR, et al. Docetaxel plus prednisone or mitoxantrone plus prednisone for advanced prostate cancer. N Engl J Med 2004;351:1502–12.
4. Bubendorf L, Schopfer A, Wagner U, et al. Metastatic patterns of prostate cancer: an autopsy study of 1,589 patients. Hum Pathol 2000;31:578–83.
5. Nelson WG, De Marzo AM, Isaacs WB. Prostate cancer. N Engl J Med 2003;349:366–81.
6. Hsing AW, Chokkalingam AP, Gao YT, et al. Allium vegetables and risk of prostate cancer: a population-based study. J Natl Cancer Inst 2002;94:1648–51.
7. El-Bayoumy K, Sinha R, Pinto JT, Rivlin RS. Cancer chemoprevention by garlic and garlic-containing sulfur and selenium compounds. J Nutr 2006;136:864–9S.
8. Unnikrishnan MC, Kuttan R. Tumour reducing and anticarcinogenic activity of selected spices. Cancer Lett 1990;51:85–9.
9. Riggs DR, DeHaven JI, Lamm DL. *Allium sativum* (garlic) treatment for murine transitional cell carcinoma. Cancer 1997;79:1987–94.
10. Marsh CL, Torrey RR, Woolley JL, Barker GR, Lau BH. Superiority of intravesical immunotherapy with *Corynebacterium parvum* and *Allium sativum* in control of murine bladder cancer. J Urol 1987;137:359–62.
11. Lau BH, Woolley JL, Marsh CL, Barker GR, Koobs DH, Torrey RR. Superiority of intralesional immunotherapy with *Corynebacterium parvum* and *Allium sativum* in control of murine transitional cell carcinoma. J Urol 1986;136:701–5.
12. Uda N, Kashimoto N, Sumioka I, Kyo E, Sumi S, Fukushima S. Aged garlic extract inhibits development of putative preneoplastic lesions in rat hepatocarcinogenesis. J Nutr 2006;136:855–60S.
13. Katsuki T, Hirata K, Ishikawa H, Matsuura N, Sumi S, Itoh H. Aged garlic extract has chemopreventative effects on 1,2-dimethylhydrazine-induced colon tumors in rats. J Nutr 2006;136:847–51S.
14. Tanaka S, Haruma K, Yoshihara M, et al. Aged garlic extract has potential suppressive effect on colorectal adenomas in humans. J Nutr 2006;136:821–6S.
15. Amagase H, Petesch BL, Matsuura H, Kasuga S, Itakura Y. Intake of garlic and its bioactive components. J Nutr 2001;131:955–62S.
16. Lawson LD, Wang ZJ. Pre-hepatic fate of the organosulfur compounds derived from garlic (*Allium sativum*). Planta Med 1993;59 (Suppl.):A688–9.
17. Xiao D, Pinto JT, Soh JW, et al. Induction of apoptosis by the garlic-derived compound *S*-allylmercaptocysteine (SAMC) is associated with microtubule depolymerization and c-Jun NH(2)-terminal kinase 1 activation. Cancer Res 2003;63:6825–37.
18. Shirin H, Pinto JT, Kawabata Y, et al. Antiproliferative effects of *S*-allylmercaptocysteine on colon cancer cells when tested alone or in combination with sulindac sulfide. Cancer Res 2001;61:725–31.
19. Pinto JT, Qiao C, Xing J, et al. Alterations of prostate biomarker expression and testosterone utilization in human LNCaP prostatic carcinoma cells by garlic-derived *S*-allylmercaptocysteine. Prostate 2000;45:304–14.
20. Pinto JT, Qiao C, Xing J, et al. Effects of garlic thioallyl derivatives on growth, glutathione concentration, and polyamine formation of human prostate carcinoma cells in culture. Am J Clin Nutr 1997;66:398–405.
21. Hu X, Cao BN, Hu G, He J, Yang DQ, Wan YS. Attenuation of cell migration and induction of cell death by aged garlic extract in rat sarcoma cells. Int J Mol Med 2002;9:641–3.
22. Chu Q, Ling MT, Feng H, et al. A novel anticancer effect of garlic derivatives: inhibition of cancer cell invasion through restoration of E-cadherin expression. Carcinogenesis 2006;27:2180–9.
23. Rhodes DR, Sanda MG, Otte AP, Chinnaiyan AM, Rubin MA. Multiplex biomarker approach for determining risk of prostate-specific antigen-defined recurrence of prostate cancer. J Natl Cancer Inst 2003;95:661–8.
24. Larue L, Bellacosa A. Epithelial-mesenchymal transition in development and cancer: role of phosphatidylinositol 3′ kinase/AKT pathways. Oncogene 2005;24:7443–54.
25. Cheung HW, Chun AC, Wang Q, et al. Inactivation

of human MAD2B in nasopharyngeal carcinoma cells leads to chemosensitization to DNA-damaging agents. Cancer Res 2006;66:4357–67.

26. Yang M, Jiang P, Sun FX, et al. A fluorescent orthotopic bone metastasis model of human prostate cancer. Cancer Res 1999;59:781–6.

27. Sumioka I, Matsura T, Kasuga S, Itakura Y, Yamada K. Mechanisms of protection by *S*-allylmercaptocysteine against acetaminophen-induced liver injury in mice. Jpn J Pharmacol 1998;78:199–207.

28. Hoffman RM. Orthotopic metastatic mouse models for anticancer drug discovery and evaluation: a bridge to the clinic. Invest New Drugs 1999;17:343–59.

29. Singh AS, Figg WD. *In vivo* models of prostate cancer metastasis to bone. J Urol 2005;174:820–6.

30. Berezovskaya O, Schimmer AD, Glinskii AB, et al. Increased expression of apoptosis inhibitor protein XIAP contributes to anoikis resistance of circulating human prostate cancer metastasis precursor cells. Cancer Res 2005;65:2378–86.

31. Pchejetski D, Golzio M, Bonhoure E, et al. Sphingosine kinase-1 as a chemotherapy sensor in prostate adenocarcinoma cell and mouse models. Cancer Res 2005;65:11667–75.

32. Yang M, Baranov E, Jiang P, et al. Whole-body optical imaging of green fluorescent protein-expressing tumors and metastases. Proc Natl Acad Sci U S A 2000;97:1206–11.

33. Sava T, Basso U, Porcaro A, Cetto GL. New standards in the chemotherapy of metastatic hormone-refractory prostate cancer. Expert Rev Anticancer Ther 2005;5:53–62.

34. Kohya N, Kitajima Y, Jiao W, Miyazaki K. Effects of E-cadherin transfection on gene expression of a gallbladder carcinoma cell line: repression of MTS1/S100A4 gene expression. Int J Cancer 2003;104:44–53.

35. Nam JS, Ino Y, Kanai Y, Sakamoto M, Hirohashi S. 5-Aza-2′-deoxycytidine restores the E-cadherin system in E-cadherin-silenced cancer cells and reduces cancer metastasis. Clin Exp Metastasis 2004;21:49–56.

36. Glinskii AB, Smith BA, Jiang P, et al. Viable circulating metastatic cells produced in orthotopic but not ectopic prostate cancer models. Cancer Res 2003;63:4239–43.

37. Loric S, Paradis V, Gala JL, et al. Abnormal E-cadherin expression and prostate cell blood dissemination as markers of biological recurrence in cancer. Eur J Cancer 2001;37:1475–81.

38. Zieglschmid V, Hollmann C, Bocher O. Detection of disseminated tumor cells in peripheral blood. Crit Rev Clin Lab Sci 2005;42:155–96.

39. Deryugina EI, Quigley JP. Matrix metalloproteinases and tumor metastasis. Cancer Metastasis Rev 2006;25:9–34.

40. Sigounas G, Hooker J, Anagnostou A, Steiner M. *S*-allylmercaptocysteine inhibits cell proliferation and reduces the viability of erythroleukemia, breast, and prostate cancer cell lines. Nutr Cancer 1997;27:186–91.